Advanced Fiber Materials (2023) 5:138–153
https://doi.org/10.1007/s42765-022-00200-4

RESEARCH ARTICLE

Bioinspired Stable Single-Layer Janus Fabric with Directional Water/Moisture Transport Property for Integrated Personal Cooling Management

Yifan Si[1] · Shuo Shi[1] · Zhichao Dong[2] · Hanbai Wu[1] · Fengxin Sun[3] · Jieqiong Yang[1] · Jinlian Hu[1]

Received: 6 June 2022 / Accepted: 25 August 2022 / Published online: 6 October 2022

Abstract

Extensive progress has been achieved regarding Janus fabric for directional water transport due to its excellent and feasible personal cooling management ability, which has great significance for energy conservation, pollution reduction, and human health. However, existing Janus asymmetric multilayer fabrics for directional water transport are still limited by their complicated syntheses and poor stabilities. Inspired by the compositionally graded architecture of leaf cuticles, we propose a single-layer Janus personal cooling management fabric (JPCMF) via a one-step electrospinning method. The JPCMF shows not only great directional bulk water transport ability but also asymmetry moisture (water vapor) transport ability with a high asymmetry factor (1.49), water vapor transmission value (18.5 kg^{-1} m^{-2} D^{-1}), and water evaporation rate (0.735 g h^{-1}). Importantly, the JPCMF exhibits outstanding durability and stability thanks to a novel electrostatic adsorption-assisted self-adhesion strategy for resisting abrasion, peeling and pulling. With these characteristics, the JPCMF can achieve a 4.0 °C personal cooling management effect, better than taht of cotton fabric, on wet skin. The good biocompatibility and nontoxicity also endow the JPCMF with the potential to be a self-pumping dressing. Our strategy should facilitate a new method for developing next-generation intelligent multifunctional fabrics.

Keywords Cooling management · Janus, directional transport · Electrospinning · Superwettability, bioinspired

Introduction

With the intensification of the greenhouse effect caused by human industrial activities and environmental damage, extreme heat climate can lead to respiratory problems, cardiovascular disease, metabolic disorders and even human death, which, in turn, enhances human reliance on energy-intensive and polluting refrigeration equipment, thus creating a vicious circle [1–4]. With this also comes a number of economic and psychological problems that not only negatively influence carbon–neutral strategic objectives but also disturb the stability of labor productivity. An energy-free "air-conditioning" fabric for personal cooling management (PCM) that can control the microclimate of human skin will be the most effective way to overcome this dilemma [4–9]. At present, PCM fabric research has three major popular topics: Janus fabric for directional water transport [10–15], passive radiative cooling fabric [5, 16–19] and self-pore adjustment fabric [20–22]. However, the latter two are still in the laboratory stage because of problems of limited efficiency and poor controllability [17, 20–22]. Janus fabric for directional water transport with asymmetric wettability can extract the sweat rapidly from human skin and transport it to the outer environment with a high evaporation rate to remove excess heat. This emerging strategy is the most promising method for practical application due to its advantages of an easy large-area preparation and high efficiency [23–26], which has attracted the attention of many researchers and institutions.

Yifan Si and Shuo Shi have contributed equally to the work.

✉ Jinlian Hu
jinliahu@cityu.edu.hk

[1] Department of Biomedical Engineering, City University of Hong Kong, Hong Kong S.A.R 999077, China

[2] CAS Key Laboratory of Bio-Inspired Materials and Interfacial Sciences, Technical Institute of Physics and Chemistry, Chinese Academy of Sciences, Beijing 100190, China

[3] Key Laboratory of Eco-Textiles of Ministry of Education, Jiangnan University, Wuxi 214122, China

Unfortunately, almost all of the reported Janus fabrics for directional water transport have been designed by asymmetric multilayer structures to obtain wettability/morphology gradient driving liquids across the "diode-like" fabric directionally [11, 12, 24, 27, 28]. This design inevitably leads to an extremely weak binding force between layers, especially for hydrophilic and hydrophobic layers, which seriously restricts the practical application of Janus fabric for directional water transport. If the binding force between layers is enhanced by subsequent physical or chemical treatments, it will not only increase the complexity of the preparation process and reduce the controllability but also increase the preparation cost. Consequently, the development of a stable single-layer Janus fabric for directional water transport for PCMs via a one-step method is very meaningful for actual daily-life applications. Single-layer Janus fabric can be obtained by hydrophobic treatment of one side of ready-made superhydrophilic fabrics [12, 13]. However, it remains a challenge to simultaneously realize the unification of fabric preparation and Janus wettability regulation. On the other hand, it is worth noting that past relevant studies only focused on the directional transport performance of bulk water (water droplets) [10, 13, 24, 25, 27, 29, 30], but ignored the asymmetric directional transport of moisture (water vapor). In fact, during outdoor physical work or sports, a large amount of water vapor will be released from the human body along with sweat. If the directional transport of bulk water and water vapor can be realized simultaneously, it will surely enhance the heat dissipation ability of the fabric with respect to the human body with a better PCM effect [25, 31–34]. A recent study demonstrated that the asymmetric transport of moisture can permeate through astomatous olive and ivy leaf cuticle directions due to the polarity gradient regulated by its outer hydrophobic waxes and inner hydrophilic polysaccharides (Fig. 1a) [35]. By regulating the hydration level, leaves can control the direction of asymmetric moisture transport in different humidity environments, allowing plants to better adapt to their environment and survive. To improve the comfort of human living in different humidity/temperature environments, Janus fabrics with bulk/vapor water directional transport performance for highly efficient PCMs will be one of the main development directions of the next generation of intelligent fabrics.

Herein, inspired by the compositionally graded architecture of leaf cuticles, we propose a single-layer Janus personal cooling management fabric (JPCMF) via a one-step rapid electrospinning method. By means of a novel electrostatic adsorption-assisted self-adhesion strategy, our JPCMF exhibits asymmetric wettability and outstanding durability through the fixation of superhydrophobic nanoparticles on a single side of superhydrophilic fibers. Furthermore, our JPCMF shows a directional bulk water transport ability and an asymmetric moisture (water vapor) transport ability with a high asymmetry factor. Under the resulting synergistic effect, the water vapor transmission (WVT) and water evaporation rate of the JPCMF both reach great values, resulting in excellent PCM ability with respect to wet skin. This decrease in temperature is approximately 4.0 ℃ lower than that of cotton fabrics. The JPCMF also displays good biocompatibility and nontoxicity. These results illustrate that the JPCMF has a splendid PCM effect and can be used for the next generation of intelligent clothing and functional dressings.

Results and Discussion

Design and Characterization of the JPCMF

The stable single-layer Janus personal cooling management fabric (JPCMF) was rapidly formed with the aid of a single-needle electrospinning device (Fig. 1b). Large area JPCMFs with good tailorability can be prepared by this method (Fig. 1c and Fig. S1). Briefly, a thermoplastic polyurethane (TPU)/microcrystalline cellulose (MCC) solution is loaded into the injection syringe [24, 36–40]. Under the excitation of high voltage, the micro/nano fibers are emitted from the needle and deposited on the above receiving substrate (Fig. S2). To obtain the JPCMF in one step, receiving substrate is selected as porous gauze (Fig. S3a), and superhydrophobic silica nanoparticles (SSNs) (Fig. S3b) are uniformly spread on its surface. Under a high negative voltage, SSNs will not fall off from the gauze due to electrostatic attraction (Fig. 1d, ①). During the electrospinning process, the inner side of micro/nano fibers also interacts closely with the nanoparticles due to electrostatic attraction. Meanwhile, the process from formation to deposition is accompanied by the constant volatilization of solvents and the gradual solidification of micro/nano fibers (Fig. 1d, ②). In addition, SSNs with negative charged (Fig. S4) may interact electrostatic with TPU nanofibers emitted from the positive electrode to improve their bonding force. Specifically, when the electrospun fabric is removed from the receiving substrate, a portion of the SSNs it had made contact with will be firmly attached to its inner side, forming strong interactions that facilitate stable one-sided hydrophobicity (Fig. 1d, ③ and details in the Experimental Section).

Our electrostatic adsorption-assisted self-adhesion strategy can avoid the weak binding force caused by the multilayer structure and simplify the preparation process. Scanning electron microscopy (SEM) was conducted to observe the morphology of the two sides of the JPCMF. As shown in Fig. 1e, the hydrophobic side has some aggregated white SSNs on its surface. At high magnifications, some SSNs can be seen attached to the surface.

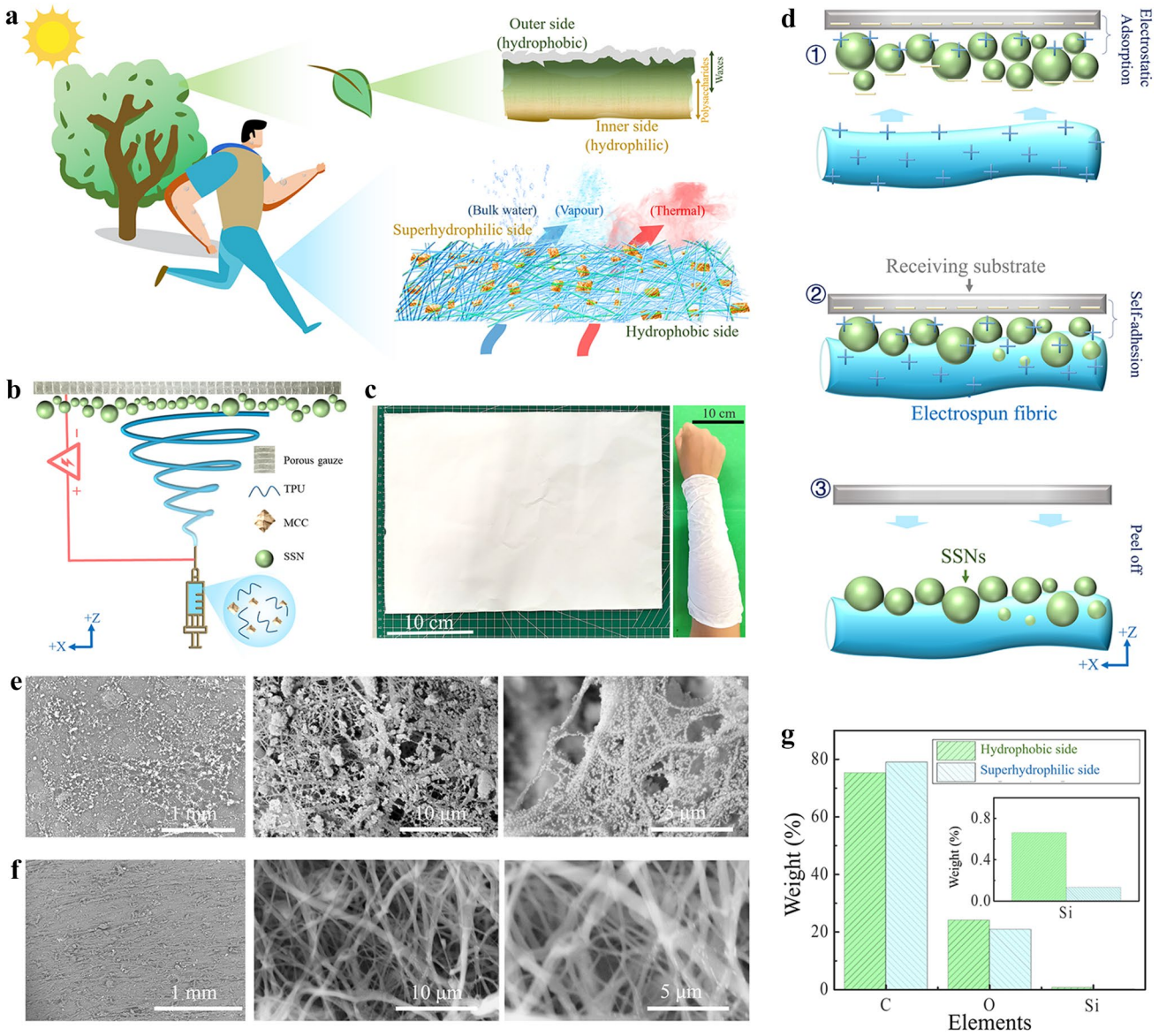

Fig. 1 Concept design and fabrication process of the Janus personal cooling management fabric (JPCMF). **a** Schematic illustrating the JPCMF with bulk water/moisture directional transport ability inspired by asymmetric leaf cuticles. **b** Schematic illustration of the single-needle electrospinning equipment. **c** Digital photograph of the large-sized JPCMF and arms wrapped in the large-sized JPCMF. **d** Schematic illustration of the self-adhesion mechanism of the JPCMF. **e–f** Different resolution SEM images of the (**e**) hydrophobic side and (**f**) superhydrophilic side of the JPCMF. **g** Content statistics of the C, O and Si elements on the hydrophobic side and superhydrophilic side, respectively. Insert: The content statistics of Si element

The superhydrophilic side is much flatter overall in low magnification images (Fig. 1f). It can also be proven by energy-dispersive spectroscopy (EDS) that superhydrophobic silica particles only exist on the hydrophobic surface, as shown in Fig. 1g and Fig. S5. In addition, the strength of the JPCMF does not decrease in the presence of SSNs (Fig. S6).

Directional Bulk Water Transport in the JPCMF

To provide insight into the wettability difference between the two sides of the JPCMF, a water droplet (5 μL) wicking/spreading process was investigated from the top view (Fig. S7). When the dyed-water droplet is deposited on the hydrophilic side (MCC content 5 wt%), it collapses into a

semicircle immediately with an instantaneous WCA of ~ 60°. The droplet then spreads out on this side and the WCA gradually drops to 0°. After 57 s, the droplets disappeared, leaving only a wetted area approximately 7.1 mm in diameter (marked by a green dotted circle). However, once the dyed-water droplet is deposited on the hydrophobic side, it maintains a decreasing spherical shape (WCA ~ 140°) with a small contact area (marked by a red dotted circle). Compared with that in the first case, the wetted area is lighter in color, indicating that the wetted area is on the downward-facing side [11, 24]. At this point, the area ratio of the upper and lower wetted areas is approximately 57.1. This asymmetric spreading process is attributed to the surface energy gradient between the two Janus sides.

The spreading time is determined by the superhydrophilicity of the JPCMF. The influence of MCC content on its hydrophilicity and liquid spreading time was investigated, and the dynamic WCA was used to characterize the process [10, 24]. The JPCMFs with MCC concentrations of 5, 10, 15, and 20 wt% are defined as JPCMF-5, JPCMF-10, JPCMF-15, and JPCMF-20, respectively. According to Fig. 2a, the WCAs of the four samples continuously decline to 0° over time until the droplets are completely spread out on the superhydrophilic side. For JPCMF-20, the droplet fully spread on the superhydrophilic side in just 1.3 s, which is 146 times faster than that of the JPCMF-5 sample. For the hydrophobic side, the droplets show a "steady disappearance" state. Its WCA value remains large for a long time, but rapidly decrease to 0° in a short period of time in the later period (except for JPCMF-5, where the droplets remained spherical for a long time, > 540 s, due to the weak hydrophilicity of the lower layer). The reason for this result is that the droplet vertically penetrates the JPCMF from the hydrophobic side and is absorbed by the superhydrophilic layer below. However, the three-phase contact line (TCL) basically does not move [12, 32]. Therefore, the wetting area of the hydrophobic side does not increase. Similarly, the penetration time of a droplet on the JPCMF-20 sample is only 5.6 s, which is 9.3 times shorter than that of JPCMF-10. Based on its Janus wettability, it is reasonable to conclude that JPCMF-20 has excellent directional bulk water transport ability.

We also carried out the directional bulk water transport experiment. As illustrated in Fig. 2b, bulk dyed-water droplets are added drop by drop to both sides of JPCMF-20. Even as much as 0.3 mL of bulk water can stand on the small and thin JPCMF (superhydrophilic side upward). Conversely, when the hydrophobic side is up, the bulk water penetrates JPCMF-20 and eventually drips down. Although some mechanism models have been proposed in previous studies [28], it has been suggested that the ability of liquids to penetrate Janus membranes/fabrics is the result of capillary forces competing with gravity in the vertical direction [10–12, 24, 30, 41]. However, in fact, in this process, the two-dimensional horizontal capillary force is the first factor to be considered [42, 43]. It can be observed

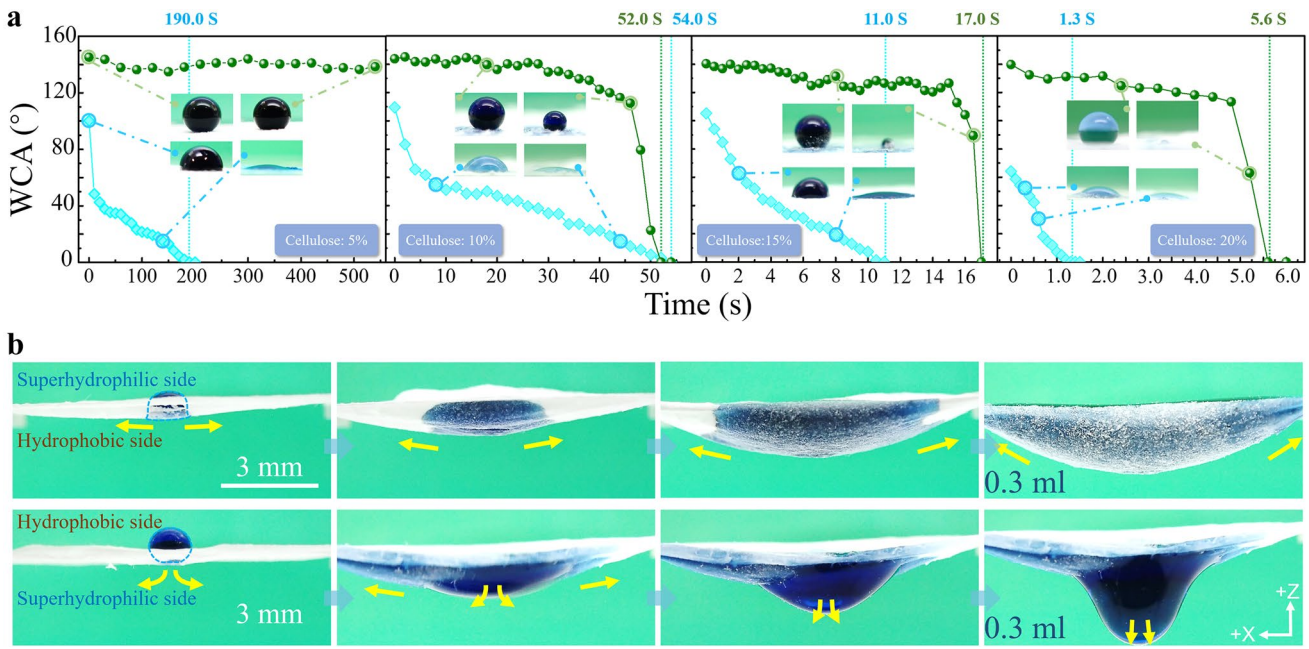

Fig. 2 Directional bulk water transport of the JPCMF. **a** Dynamic apparent water contact angles (WCAs) on the hydrophobic side (green filled circles) and superhydrophilic side (blue-filled squares) of JPCMFs with different CMM contents. Insets: the corresponding optical photographs of the blue-dyed-water droplets (20 μL). **b** Directional bulk water (0.3 mL) transport process from the side view of JPCMF-20 when the water droplets were dropped on the superhydrophilic side (top row) and hydrophobic side (bottom row) (colour figure online)

through the experiment that, no matter which side is up, the droplet will first spread in the superhydrophilic side in the two-dimensional horizontal direction, until it is completely wetted. This is caused by layer-by-layer electrospinning technology. Micro/nano fibers tend to be interleaving or interweaved laterally, rather than disorderly, during the electrospinning process. There are no clear boundaries between long fibers of the same layer. However, the different layers are connected by micro/nano pores. The micro/nano pores inside each layer cause the liquid to spread rapidly under the action of a strong capillary force, expressed as P_c ($P_c = \frac{2\gamma\cos\theta}{r_p}$, where γ, θ and r_p are the surface tension of the liquid, liquid contact angle and radius of fabric pores, respectively) [44, 45] on the two-dimensional plane. It is difficult to transport longitudinally. Until this layer is saturated, water begins to travel down the next layer through the newly formed liquid bridge, and finally, the entire superhydrophilic side is wetted (Fig. S8) [30, 42].

A schematic diagram of the directional bulk water transport in the JPCMF along the vertical direction is demonstrated in Fig. 3a, b. When the superhydrophilic side is facing upward (Fig. 3a), the water spreads out completely in the horizontal direction. Under the action of gravity, it forms a downward convex surface at the pore and is subjected to upward additional pressure. With increasing liquid volume, the curvature of the convex surface increases and the additional pressure (P_{add}) increases according to the following equation:

$$P_{add} = \frac{4\gamma\sin[\theta(\varphi) - \varphi]}{(L - 2R_{SNN}) + 2R_{SNN}(1 - \sin\varphi)}, \quad (1)$$

where L is the distance between adjacent SSNs, R_{SNN} is the radius of the SSNs, $\theta(\varphi)$ is the local contact angle and φ is

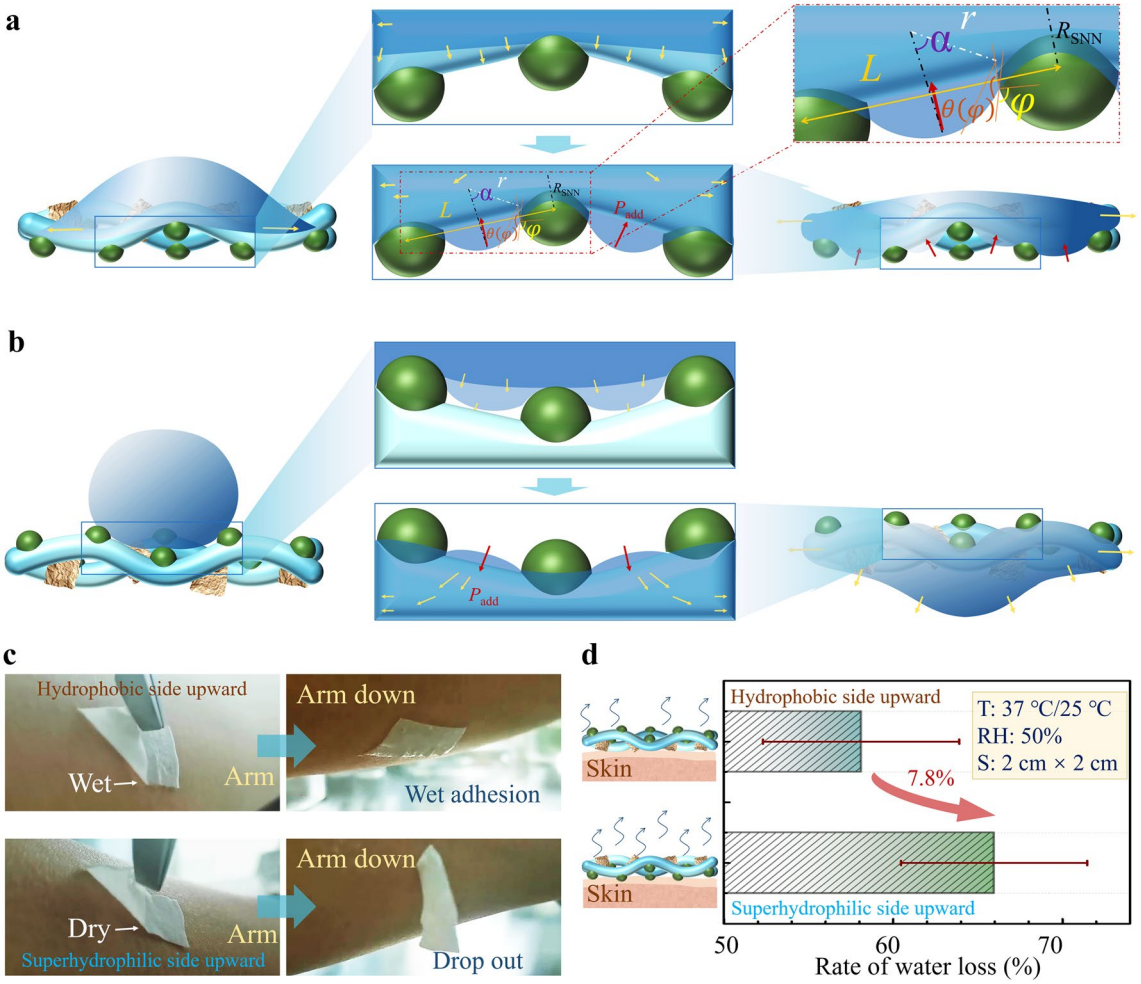

Fig. 3 Mechanisms and results of the directional bulk water transport. **a**, **b** Schematics displaying the directional bulk water transport mechanism of JPCMF-20. **c** Optical photographs show the asymmetric wet/dry adhesion results between superhydrophilic side (top row) or hydrophobic side (bottom row) of JPCMF-20 with wet skin. **d** Evaporation rate of the water test showing that when the superhydrophilic layer contacts the skin, the evaporation rate of water on the wet fabric surface is much lower than that when the hydrophobic side is inwards

the local geometrical angle [28, 30, 46]. However, because air is a completely superhydrophobic medium (WCA ~ 180°), the liquid cannot be pulled by vertical capillary forces, so it can only remain on at the top of the JPCMF-20. The experimental results show that the more hydrophobic the fabric is, the more water it can stand. The WCA of the hydrophobic side of the JPCMF-20 is very high (> 140°), so it can withstand large amounts of bulk water. In contrast, when the liquid touches the hydrophobic side, a downward convex surface also forms under the action of gravity, and the curvature of the convex surface will increase with increasing liquid volume (Fig. 3b). Although the additional pressure is still upward, the difference is that once the convex surface touches the superhydrophilic side below, it is attracted by a huge capillary force that creates a channel for the liquid to penetrate through. Once this transformation is completed, the convex surface will turn upward, and the water will be subjected to additional downward pressure, which accelerates directional bulk water transport due to this push–pull effect. Apparently, the liquid penetrates the hydrophobic side and wets the superhydrophilic side. Eventually, as the volume of bulk water increases, gravity takes over again, and the excess droplets fall drop by drop. Thus, the thinner the hydrophobic layer is, the more conducive it is to the realization of directional water transport in the Janus fabric. Our electrostatic adsorption-assisted self-adhesion strategy has the advantage of constructing a discontinuous hydrophobic layer to achieve the unity of high-hydrophobicity and directional bulk water transport ability.

Heavy physical work, strenuous exercise, or sweltering weather can cause the human body to eliminate a large amount of sweat to maintain the body's normal metabolism and prevent abnormal body disorders. The typical application purpose of directional transport fabric is spontaneous sweat extraction to keep the body cool and comfortable [24, 27]. JPCMF-20 can act as a second functional skin to achieve this purpose. A control experiment using water to simulate skin sweat was established in this study. When the superhydrophilic side of JPCMF-20 comes into direct contact with the skin, the water is absorbed by the superhydrophilic side, but the wet adhesion between JPCMF-20 and the skin causes JPCMF-20 to stick to the skin and prevents it from detaching naturally, even when the arm is facing down to the ground (Fig. 3c). However, when hydrophobic side of the JPCMF is in direct contact with the wet skin, the situation is completely different. Because of the excellent directional water transport ability of JPCMF-20, the water on the skin will penetrate through the hydrophobic side and is absorbed by the outer superhydrophilic layer. JPCMF-20 remains dry with little adhesion to the skin [10]. When the arm is facing down, the wetted JPCMF-20 is easily detached from the arm under the action of gravity, making the body more comfortable. More importantly, an asymmetric water volatilization rate is found between the two cases (Fig. 3d). The preliminary experimental results reveal that, under the same environmental conditions (skin temperature ~ 36 ℃, environment temperature ~ 25 ℃, relative humidity ~ 70%), when the superhydrophilic layer contacts the skin, the evaporation rate of water on the wet fabric surface is 7.8% lower than that when the hydrophobic side is inwards, which indicates that JPCMF-20 presents a desirable asymmetric moisture management ability.

Asymmetric Moisture Transport in the JPCMF

In recent research on Janus fabric or membranes, it is not difficult to find that the directional transport of bulk water (using droplets to simulate sweat) has been demonstrated as one of its basic abilities [10, 11, 23, 24, 27]. However, in real-world applications, it is common for people to encounter moisture escaping from their skin without sweat formation, especially in muggy weather or when they are gently exercising in cold weather. In these situations, achieving the asymmetrical moisture (water vapor) transport through fabric is very important to maintain the wearer's comfort and cool. Unfortunately, there are almost no studies on the asymmetric moisture transport of Janus fabric [13, 26]. A recent study revealed the asymmetric moisture transport through astomatous olive and ivy leaf cuticles [35]. Inspired by this phenomenon and method, we revealed that the JPCMF-20 also has an asymmetric moisture transport ability, and carried out a theoretical analysis of the results.

These asymmetric moisture transport characteristics were investigated as a function of temperature (T), relative humidity (RH) and fabric wettability using the inverted wet-cup method. The schematic (not to scale, Fig. 4a) representation of the gravimetric inverted wet-cup method was used to determine the moisture transport ability from both sides of JPCMF-20 (thickness, 56 ± 4 μm). In a sealed constant-temperature humidity chamber with controlled wind speed, a cup filled with water is suspended upside down in the middle, and the cup mouth is sealed by the JPCMF-20. Since the interior of the cup is a relatively high humidity environment (RH ~ 100%), the liquid will evaporate outward and the quality will be reduced. As a proof-of-concept, the amount of water lost in the cup over a constant period is defined as the water vapor transmission (WVT) value [10, 33, 47]. The asymmetric moisture transport characteristics of the JPCMF can be expressed by an asymmetry factor (F), defined as the ratio of the WVT measured in the two directions under the same conditions ($F = \frac{WVT(\text{hydrophobicsideupward})}{WVT(\text{superhydrophilicsideupward})}$).

The effects of different RH and T values on the asymmetry factor (F) were systematically studied in detail. Figure 4b–e shows that with increasing T, under the same RH conditions, the WVT value increases significantly,

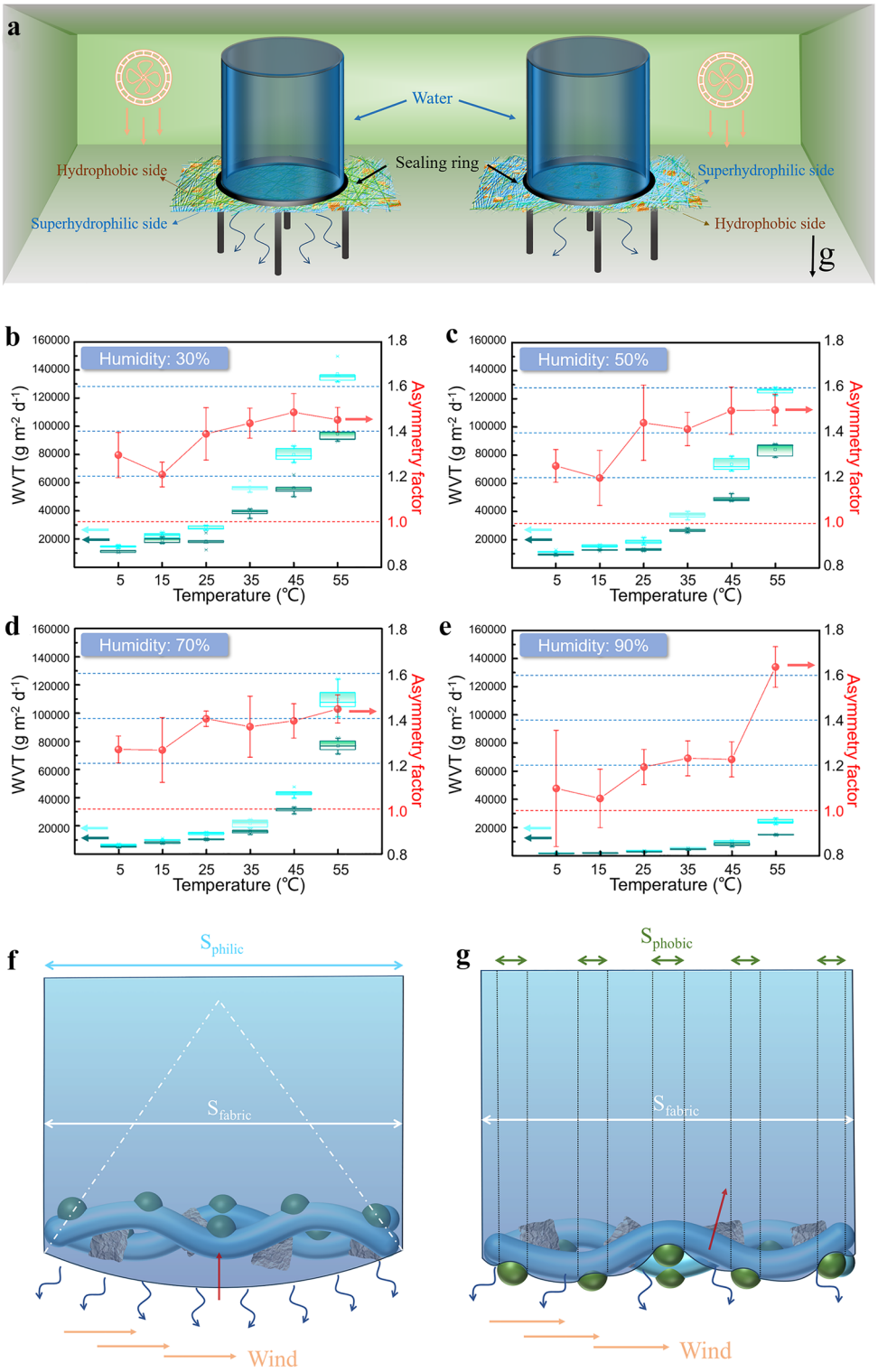

Fig. 4 Asymmetric moisture transport of JPCMF-20. **a** Schematic (not to scale) of the gravimetric inverted wet-cup method to determine the WVT of JPCMF-20 from both sides under various environmental conditions. **b–e** Measurement results of the asymmetry factor (*F*) (red filled dot) and box plots of the WVT values of JPCMF-20 (green box, hydrophobic side outward; blue box, superhydrophilic side outward; $n = 5$) under various environmental conditions. **f–g**, Schematics displaying the asymmetric moisture transport mechanism on JPCMF-20 (colour figure online)

regardless of whether the outside is hydrophobic or superhydrophilic. Because the movement of water molecules is intensified, they tend to diffuse to the outer side towards the low humidity. Under standard test conditions (RH = 50%, T = 25 ℃), the WVT values of the two directions are 18.5 kg^{-1} m^{-2} D^{-1} (superhydrophilic side outward) and 12.8 kg^{-1} m^{-2} D^{-1} (hydrophobic side outward). As expected, with the increase of RH, under the same T condition, the WVT value will decrease obviously whether the outside is hydrophobic or superhydrophilic. The greater the RH of the air is, the greater the actual pressure of water vapor, and the closer it is to the saturation vapor pressure at the same temperature, resulting in slower moisture transport.

What is more worthy of analysis and attention is the asymmetry factor F of direction determination. When the RH is maintained at a low or medium level (RH < 90%, Fig. 4b–d), the asymmetry factor F will gradually rise from 1.2 at low temperatures to 1.5 at high temperatures. The results indicate that the JPCMF-20 can be a great choice for functional sportswear. When its hydrophobic surface touches human skin, it not only transport sweat to the outside, but the moisture emitted by the body is also more inclined to transport outwardly to make a person feel cool and comfortable. The higher the external temperature is, the more obvious this asymmetry effect will be.

The different wetting modes of the outside under two different directions are the root cause of this result. When the superhydrophilic side is facing outward (Fig. 4f), it will be completely wetted. In this case, the effective volatile area (S_{philic}) is completely consistent with the entire area of the JPCMF-20 (S_{fabric}). When the hydrophobic side is facing outward (Fig. 4g), the water cannot wet the outside and contact the air directly. Moreover, the transport of the moisture will be blocked by the hydrophobic fiber and it can only diffuse outwardly through the micro/nano pores. Therefore, the actual volatile area (S_{phobic}) is far less than S_{fabric}, that is, $S_{phobic} < S_{philic}$. Therefore, in the case of high RH and low T (RH = 90%, T = 5 and 15 ℃, in Fig. 4e), because the WVT value is in a very low range, the asymmetry difference caused by the effective volatile area difference is not insignificant, and when the temperature rises, F will significantly and rapidly increase. Another key influencing factor is the wind speed of the external environment. The airflow (wind) reduces the density of water molecules on the surface, lowering the vapor pressure and accelerating evaporation. However, when the hydrophobic side is outward, due to the obstruction of the fabric, the airflow has difficulty entering the inner pores of the fabric, so the influence on the density of water molecules on the liquid surface is greatly reduced, and the volatilization of water will be slowed down. When the superhydrophilic side is outwards, the wind is in direct contact with the liquid surface (Fig. S9). To verify this interpretation, WVT values were measured with and without air flow (Fig. S10). It should be noted that the liquid will form a convex surface of different curvatures on the outside under these two situations. According to Kelvin's equation, $(\ln\frac{p_{act}}{p_{sat}} = \frac{2\gamma V_m}{rR_{con}T}$, where p_{act} is the actual vapor pressure, p_{sat} is the saturated vapor pressure of the flat surface, V_m is the molar volume of the liquid, R_{con} is the universal gas constant, and r is the radius of the droplet), a liquid with a larger radius of curvature has a lower saturated vapor pressure and is less likely to evaporate into the air. By measuring the WVT values at different heights of the water columns (Fig. S11), it can be concluded that the negative effect caused by different curvatures is very small. Especially when used as clothing, there is almost no hydrostatic pressure, resulting in the difficult formation of convex surface. It can also be inferred from Fig. 4b–e that the JPCMF-20 is especially suitable for summers with high temperatures. When the temperature is greater than 25 ℃, the F can generally be maintained at approximately 1.4. This is a good way to increase the rate at which water evaporates out of the body to take more heat away from the wearer. Of course, there may be some decrease in extremely humid conditions (RH > 90%). When the temperature is comfortable in spring and autumn (5–15 ℃), F will drop to approximately 1.2, which can reduce the asymmetric transmission to a certain extent. Generally, the asymmetric moisture transport ability of JPCMF-20 can be applicable in most conditions and seasons of daily life.

Performance Comparison

Directional transport fabric and waterproof breathable fabric are two kinds of the most representative functional personal cooling management/protection fabric [25, 34, 48, 49]. Water evaporation rate and water vapor transmission (WVT) values are used to characterize the moisture permeability and the quick-drying performance of these two fabrics, respectively. A comparison of these two values among our prepared JPCMF-20 and other reported typical references is illustrated in Fig. 5a. Compared with that of the waterproof breathable fabric [31–34, 47, 49], the WVT value of our prepared JPCMF-20 is significantly higher than that of the products reported thus far (in Fig. 5a, circular marks). This is because most of the waterproof breathable fabrics have very high WCAs. Therefore, water vapor can only be transported outward slowly through micro/nanopores. However, JPCMF-20 displays a completely wet contact water vapor model. The water evaporation rate (0.735 g h^{-1}) of JPCMF-20 is also at a higher level than that reported for directional transport fabric (in Fig. 5a, triangular marks) and it is noteworthy that all of them are multilayer structures [10–12, 23–25, 50–52]. This result indicates that our JPCMF-20 exhibits a superior

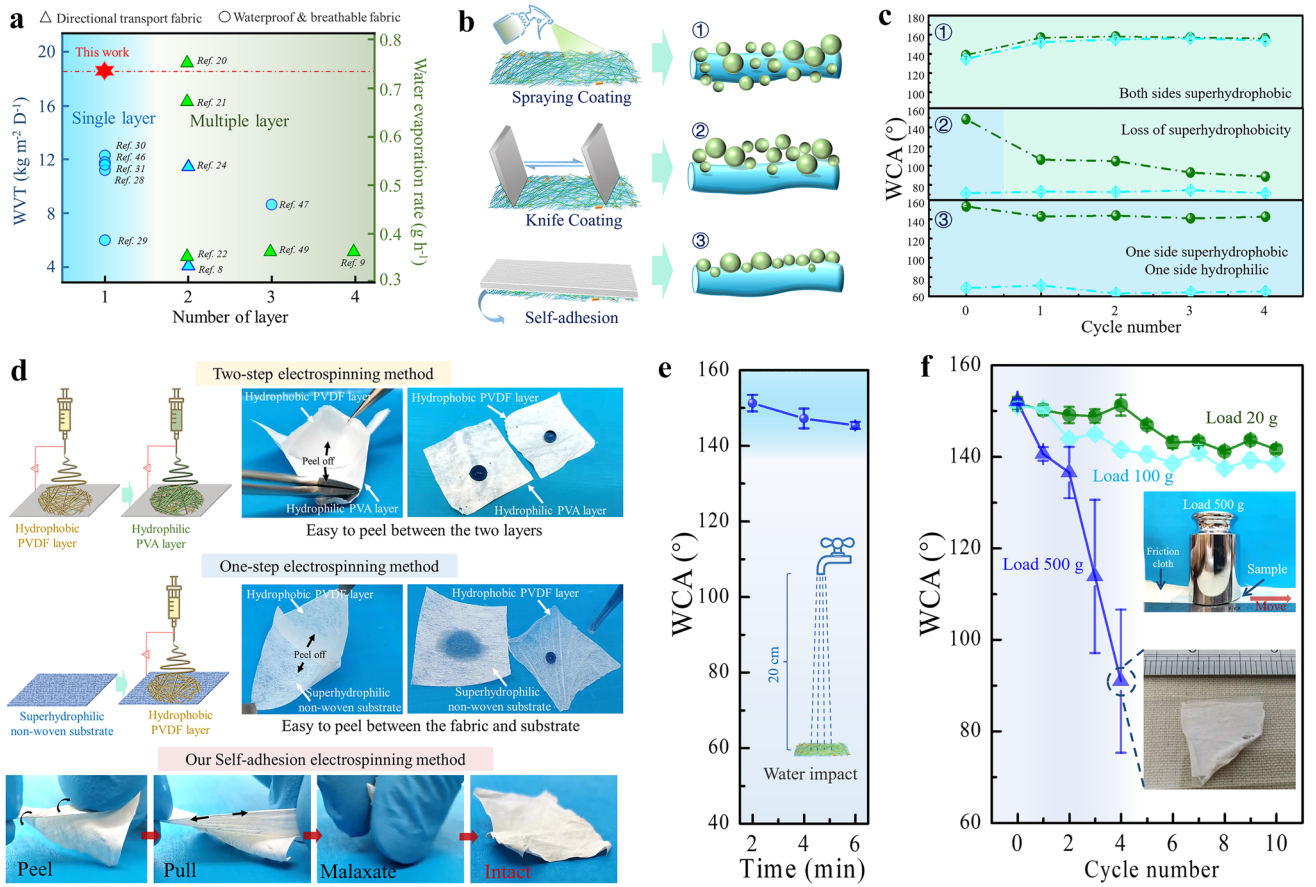

Fig. 5 Comparison of performance. **a** Relative range of the number of layers, WVT (blue marks) or water evaporation rate (green marks) of some typical directional transport fabrics (triangular marks), waterproof & breathable fabrics (circular marks) and this work (red hexagram). **b** Schematic diagrams for preparing the JPCMF via three different simple methods and the corresponding structure. **c** WCA changes of the two sides of the JPCMF obtained via three different methods with the number of cycles of ultrasonic washing. Green-filled dots and blue-filled squares represent the hydrophobic side and superhydrophilic side, respectively. The green and blue areas represent directional bulk water transport that can and cannot be achieved under this cycle number, respectively. **d** Stability of JPCMF compared with two different kinds of multilayer electrospinning fabrics. Traditional multilayer electrospinning fabrics are easy to peel and separate, but the JPCMFs can be peeled, pulled, and malaxated to remain intact. **e** Broken line graph of the WCAs after the water column impact test of the JPCMF. **f** Broken line graph of the WCAs after 0–10 abrasion cycles of the JPCMF under different loads (20 g, 100 g, and 500 g). Inset: Optical images of the abrasion test and the JPCMF after 4 abrasion cycles under a 500 g load (colour figure online)

evaporation rate with high application potential as an integrated personal cooling management fabric. It is noted that different testing methods can cause significant differences in the results. For a clearer comparison of the results, the specific values and test methods are shown in Table S1.

The weak mechanical stability caused by the multilayer structure of existing Janus fabrics for directional transport is a major challenge in this field [43, 53–56]. By virtue of the electrostatic adsorption-assisted self-adhesion strategy, our JPCMF-20 can eliminate the problem of the weak internal binding force of multilayer fabric. The spraying coating method and the dry knife coating method are two simple and common method for constructing Janus fabric and were used as control experiments here. Using a spraying coating method (Fig. 5b), an ethanol dispersion of SSNs is sprayed onto one side of the superhydrophilic pure electrospun TPU fabric to prepare superhydrophobic–hydrophilic Janus fabric. However, the fabric is completely wetted by the coating. Therefore, the SSNs are evenly dispersed inside and outside the fabric, resulting in both sides being superhydrophobic without directional water transport ability (Fig. 5c). However, the dry knife coating method can ensure that SSNs only exist on one side of the superhydrophilic pure electrospun TPU fabric (Fig. 5b), so that it has asymmetric superhydrophobic–superhydrophilic wettability. In this initial state, the Janus superhydrophobic–superhydrophilic fabric has directional water transport ability (Fig. 5c). Then, three different fabric samples are placed into ethanol/water mixture solution for ultrasonic cleaning to determine their stability (details in the Experimental Section). The results show that

the two-sided WCAs of the fabric prepared by the spraying method increase after ultrasonication. This means that its superhydrophobicity is further enhanced. We speculate that in the drying and curing process of electrospinning fiber, the fiber and SSNs will form a strong binding effect. During the ultrasonic process, the internal SSNs migrate outward, which enhances their superhydrophobicity. Obviously, the fabric obtained by the spraying method still does not have directional water transport ability, even after 4 cycles. For the Janus fabric obtained by the knife coating method, fluffy SSNs only exist on the surface, so they cannot resist the damage caused by ultrasound. As shown in Fig. 5c, after only one cycle, the WCA of its superhydrophobic surface drops to 110° from 150°, resulting in the loss of its directional water transport ability. After more cycles, the WCA decreases further until the value is almost equal to that of the hydrophilic side. However, even after multiple ultrasonic cycles, the WCA of the high-hydrophobicity side of the JPCMF prepared by the electrostatic adsorption-assisted self-adhesion strategy almost did not decrease, so it retained excellent directional water transport ability. This indicates that SSNs are firmly deposited on the fiber surface due to fiber adhesion and solidification during the process of electrospinning (Fig. S12and S13).

To further demonstrate the advantages of the single-layer structure, we carried out strength/durability test experiments. Both control samples were Janus multilayer fabrics prepared by electrospinning. Without further treatment, both multilayers are very easy to separate and eventually lose their usefulness (Fig. 5d). However, our JPCMF remains firmly intact after being peeled, pulled, and malaxated. The stability of the hydrophobic side of the JPCMF was verified by water column impact and friction experiments. As shown in Fig. 5e, after 6 min of water column impact, the hydrophobicity of JPCMF is still good, and the WCA is greater than 140°. An abrasion test was performed to further confirm this result. When the load is very small (20 g and 100 g), the hydrophobicity damage of ten abrasion cycles is very small. Only when the load is very high (500 g) does JPCMF damage occur after 4 abrasion cycles (Fig. 5f and details in the Experimental Section). In the simulated washing experiment, the multilayer was separated into two independent membranes after washing for one minute at 500 RPM. However, The JPCMF can withstand washing for 5 min and remain intact (Fig. S14). These experimental results prove that our electrostatic adsorption-assisted self-adhesion strategy is both feasible and effective. Our strategy provides a new method for preparing a next-generation stable superwetting surface/coating.

Thermal Management and Potential Application of the JPCMF

The ability of the JPCMF to effectively remove sweat from the skin can keep the human body more comfortable, and eliminate the risk of heat stress due to the self-cooling effect [11, 12, 24]. The self-cooling effect of the JPCMF is mainly due to its rapid water evaporation rate, which was further evaluated as follows. We used an infrared camera to measure the temperatures of the JPCMF and a commercial cotton fabric on the wet skin surface (Fig. S15). As shown in Fig. 6a, the JPCMF is in a cooler state with a low temperature of 24.8 ℃ (Sp1), which is 0.9 ℃ lower than the environmental temperature (Sp4) and 6.2 ℃ lower than wet arm's temperature (Sp3). However, the temperature of the cotton fabric is approximately 28.8 ℃ (Sp2) which is much higher (4.0 ℃) than the JPCMF's temperature and slightly higher (3.1 ℃) than the environmental temperature. The cooling thermal flux (Q) caused by water evaporation is believed to be the main reason for this result, which can be calculated as follows:

$$Q = L_{\text{water}} V\left(c_{\text{sat}} - c_v\right) M_v, \tag{2}$$

where V, L_{water} and M_v are evaporation rate, the enthalpy and the molar mass of water, respectively, and c_{sat} and c_v are the saturated and current vapor concentrations, respectively [12]. Obviously, a higher V leads to a greater Q. The high evaporation rate of the JPCMF is not the only factor leading to its excellent self-cooling effect.

Through the characterization of thermal conductivity, the thermal conductivity of the JPCMF (0.0155 W m^{-1} K^{-1}) was found to be higher than the thermal conductivity of TPU/MCC fabric without SSNs (0.0130 W m^{-1} K^{-1}). In fact, the asymmetric moisture distribution caused by asymmetric wettability further amplifies the asymmetric temperature distribution on the inside and outside of the JPCMF, thus stimulating the outward diffusion of heat. We carried out a qualitative theory analysis of this result. To further understand the physical mechanism of the excellent thermal-wet comfort in the skin microenvironment of the JPCMF, an ideal mathematical Eq. (3) expressing the evolution of temperature (T) against time (t) based on energy conservation is utilized to present the heat loss of the skin-fabric microenvironment by analyzing the heat and moisture transfer in the Janus fabric, which is assumed to be an isotropic material, and the effect of free convection in the fabrics is assumed to be negligible [57].

$$C^A \frac{\partial T}{\partial t} = \frac{\partial}{\partial x}\left(k(x,t)\frac{\partial T}{\partial x}\right) + \frac{\partial F_{out}}{\partial x} - \frac{\partial F_{in}}{\partial x} + \lambda(x,t)\eta(x,t), \tag{3}$$

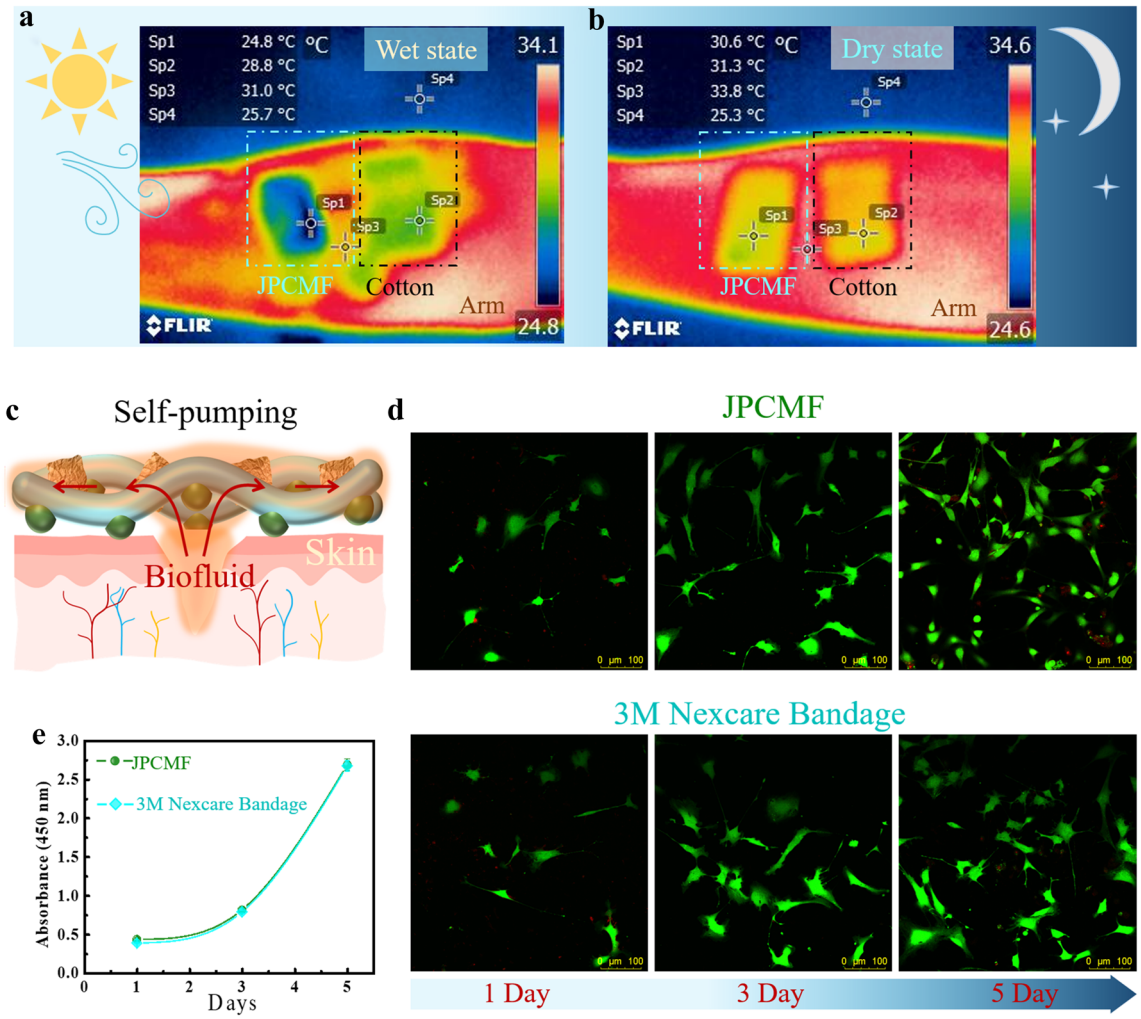

Fig. 6 Thermal management and potential application of the JPCMF. **a**–**b** Infrared camera images of the JPCMF and commercial cotton textile placed on wet (**a**) and dry skin (**b**). Sp1-Sp4 are the temperatures of JPCMF, commercial cotton textile, arm and environmental. **c**, Schematic diagram of the self-pumping dressing application of JPCMF. It can unidirectionally drain biofluid from the hydrophobic side to the superhydrophilic side. **d** Confocal fluorescence microscopy of murine fibroblast cells (NIH 3T3, ATCC) cocultured on JPCMF and 3 M Nexcare Bandage samples. for 1, 3, and 5 days, respectively. **e** Growth analysis of murine fibroblast cells (NIH 3T3, ATCC) cocultured on JPCMF and 3 M Nexcare Bandage samples for 1, 3, and 5 days, respectively (colour figure online)

where $k(x, t)$ is the effective thermal conductivity of the JPCMF, F_{out} and F_{in} represent the total thermal radiation incident toward different directions on the element along the fabric thickness (x), $\lambda(x, t)$ is the latent heat of moisture vaporization and sorption/desorption, and $\eta(x, t)$ is the water accumulation rate by moisture vaporization and sorption/desorption. The term $\frac{\partial T}{\partial x}$ actually expresses the temperature gradient of JPCMF, and this temperature gradient is considered to be approximately constant in ordinary wearing fabrics with a small evolution along the thickness; however, this changes in the JPCMF as liquid moisture mainly gathers on the superhydrophilic side, resulting in an obvious gradient moisture distribution throughout the thickness of the Janus fabric. In a simple way, the wet side of the Janus fabrics tends to show a lower temperature than the dry side due to the higher specific heat capacity of water (4.2 kJ/(kg ℃)), and thus the temperature gradient will exhibit an increased change along the fabric's thickness. Thus, $\frac{\partial^2 T}{\partial x^2}\Big|_{\text{Ordinary}} < \frac{\partial^2 T}{\partial x^2}\Big|_{\text{Janus}}$ can be obtained. In fact, the water accumulation process on the superhydrophilic side of the JPCMF can directly cause heat and moisture transfer in the fabric, which can be expressed by $\eta(x, t) = \rho\frac{\partial W_c}{\partial t}$, where W_c denotes the moisture content and ρ denotes the density of fibers. If $\frac{\partial W_c}{\partial t}\Big|_{Ordinary} < \frac{\partial W_c}{\partial t}\Big|_{Janus}$, Eq. (4) can be derived as follows:

$$\eta(x, t)|_{\text{Original}} < \eta(x, t)|_{\text{Janus}}. \tag{4}$$

By rearranging Eq. (3), the explicit expression of the heat loss in the skin-fabric microenvironment will be obtained as follows:

$$\frac{\partial T}{\partial t} = (k(t)\frac{\partial^2 T}{\partial x^2} + \lambda(x,t)\eta(x,t) + \frac{\partial F_{out}}{\partial x} - \frac{\partial F_{in}}{\partial x})(C^A)^{-1}. \quad (5)$$

The moisture in the fabrics is condensed on the fiber surface, and thus its effect on the thermal radiation is small; hence the results of $\frac{\partial F_{out}}{\partial x} - \frac{\partial F_{in}}{\partial x}$ can be treated as equal for ordinary fabrics and JPCMFs. Bearing in mind the relationship in equations and assuming the sensible heat capacity (C^A) of the fabrics to be approximately unchanged, the relationship, $\frac{\partial T}{\partial t}\Big|_{\text{Ordinary}} < \frac{\partial T}{\partial t}\Big|_{\text{Janus}}$, can be obtained. Thus, the JPCMF will have higher heat loss due to the gradient moisture distribution and large moisture accumulation rate caused by its unidirectional moisture transfer property. Therefore, the wet JPCMF can obviously and effectively reduce human skin temperature. In addition, silica nanoparticles have been proven to have a good radiation cooling ability because of the existence of surface phonon (SPh) resonance [56]. In summary, the excellent personal cooling management effect of the JPCMF is the result of a combination of many factors, which are dominated by its rapid evaporation rate and wettability gradient [57]. We also measure the temperatures of the JPCMF and the commercial cotton fabric on the dry skin surface (Fig. 6b). Visually, the temperature of the dry JPCMF (30.6 ℃) is lightly lower than that of the cotton fabric (31.3 ℃). In other words, the JPCMF does not have a significant cooling effect when the body is in a static state without perspiration, such as when sleeping at night [58]. Therefore, the JPCMF displays an intelligent integrated personal cooling management capability based on the condition of the human body.

According to the aforementioned directional transport and PCM abilities, the JPCMF sample can be used as a potential fabric for self-pumping dressing [26, 36]. Such a self-pumping dressing can unidirectionally drain excessive biofluid from the inner hydrophobic side to the outer superhydrophilic side, maintaining a dry and cool environment for faster wound healing (Fig. 6c) [13, 59, 60]. More importantly, the JPCMF shows an excellent biocompatibility similar to that of commercial dressings (3 M Nexcare Bandage). As shown in Fig. 6d–e, murine fibroblast cells (NIH 3T3, ATCC) grew well on the JPCMF sample and 3 M Nexcare Bandage (details in the Experimental Section, SI). Therefore, our samples have great potential applications in the next generation of smart dressings [28, 36]. From a practical point of view, taking into account the prices of all the ingredients, we calculated that it costs about 5–6 ¥ (~ 1 $) to produce 1 m^2 JPCMF, which can satisfy the consumption power of the vast majority of people.

Conclusions

To conclude, by taking advantage of an electrostatic adsorption-assisted self-adhesion strategy, a single-layer Janus personal cooling management fabric (JPCMF) was prepared by rapid one-step electrospinning. The JPCMF achieves directional bulk water transport and asymmetric moisture (water vapor) transport abilities simultaneously, which contribute to the high water vapor transmission values and water evaporation rates of the JPCMF, resulting in a great PCM ability in the wet state. Due to its excellent biocompatibility, our JPCMF will open up new avenues for the futuer development of intelligent clothing and functional dressings.

Experimental Section

Materials

Microcrystalline cellulose (MCC, ~ 20 μm) and lithium chloride (LiCl, ACS Reagent) were purchased from Sigma-Aldrich Co. Ltd. in Hong Kong SAR, China. N, N-dimethylformamide (AR) was purchased from Shanghai Aladdin Biochemical Technology Co., Ltd, China. Superhydrophobic silica nanoparticles (SSNs) were purchased from Regent Science Industry Limited. Gauze and 3 M Nexcare Bandage were obtained from the local market. TPU was prepared during our group's previous work.[40] All other chemicals were analytical-grade reagents and used as received. Millipore water (resistivity ~ 18 MΩ cm)) was used throughout this study.

Fabrication of Electrospinning Precursor Solution

An electrospinning precursor solution was obtained by dissolving TPU, LiCl and dispersing MCC in dimethylformamide (DMF) at 60 ℃ under constant magnetic stirring. The weight ratios of LiCl and TPU were 0.2 wt% and 20 wt%, respectively. The weight ratio of MCC was changed from 0, 5, 10, 15 to 20 wt%. After 5 h, a white, viscous, and opaque homogeneous precursor solution was obtained.

Fabrication of the Janus Personal Cooling Management Fabric

Commercial porous gauze was selected as the receiving substrate. 0.1 g superhydrophobic silica nanoparticles (SSNs) were evenly spread on the surface of gauze covering an area of 30 × 30 cm. After slight pressing, put the gauze loaded with SNNs upside down over the metal

wire and charged with a − 2 kV voltage. The as-prepared polymer solution was slowly poured into the groove, and then the groove moved back and forth on the surface of the metal wire at a uniform speed (10 cm s^{-1}) so that the polymer solution constantly sticks to the surface of the wire. Finally, the wire was charged with a high voltage of 28–30 kV, and the electrospun nanofibers were emitted from the metal wire and deposited on the surface of the gauze above. During electrospinning, the environmental temperature and relative humidity were controlled in the range of 25–28 °C and 50% respectively. The as-spun fabric was peeled off from the gauze and dried in a vacuum at 60 °C for 8–12 h. Finally, the solvent was completely volatilized and the Janus personal cooling management fabric was obtained.

Mechanical Stability Tests by Ultrasonic Cleaning

First, the tested fiber samples (5 × 5 cm) prepared by different methods were put in an oven at 60 ℃ for 2 h to remove the solvent. A cleaning solution was obtained by mixing 20 mL deionized water and 20 mL ethanol in a beaker. Clean samples to be tested were immersed in a beaker of cleaning solution until fully wetted. The beaker was placed in an ultrasonic cleaning instrument for 30 min. Next, the sample was removed and completely dried in the 60 ℃ oven for 2 h. Then the sample was emoved, and its temperature was lowered to room temperature ~ 25 ℃. The water contact angle was measured at any five positions on the sample surface. Finally, the above steps were repeated until enter the next ultrasonic cleaning cycle.

Water Column Impact Test and Abrasion Tests

A JPCMF sample (approximately 2 × 2 cm) was pasted on a clean and flat glass sheet with double-sided adhesive with the hydrophobic surface facing outwards. The sample was placed under running water. Water was dispersed on the surface and flow away with the inclination. The water flow was controlled at approximately 10 mL/s, and the distance between the sample and the outlet of the water pipe as approximately 20 cm. In the abrasion test, the JPCMF sample (approximately 2 × 2 cm) was pasted on a clean and flat glass sheet with double-sided adhesive as well, and the hydrophobic side was faced with abrasive cloth under different loads (20, 100 and 500 g). The sample was moved a distance of 10 cm along a ruler as one cycle.

Thermal Measurements of the JPCMF and Commercial Cotton Textile

This experiment was carried out in a room with a constant temperature of 25 ℃. First, a clean, dry arm was moved to a location on the table, approximately 70 cm above the ground. Then, two JPCMF and commercial cotton textile samples of similar size (~ 2 × 4 cm) were applied to the skin of the dry arm. Then, the samples were gently pressed onto the skin. One minute later, the temperature of both samples, the arm and the environment were simultaneously measured with an infrared thermal imaging camera. The camera was approximately 1 m away from the arm and the samples. Then, two samples were taken and placed on the table. Clean, room-temperature water was sprayed evenly onto the surface of the arm until the arm was completely soaked. Next, two samples were placed on the wet arms and pressed gently until the samples were completely wetted. One minute later, the temperatures of the two wet samples, the wet arm and the environment were simultaneously measured using an infrared thermal imaging camera. The camera was located approximately 1 m away from the arm and sample. The arm remained motionless and there was no obvious air movement in the environment.

Cytotoxicity and Biological Compatibility Assay of the Janus Personal Cooling Management Fabric

Murine fibroblast cells (NIH 3T3, ATCC) were used to assay the cytotoxicity of the potential biomaterials according to previous research. NIH 3T3 cells were expanded to fourth passages in growth media (10% FBS, 1% Pen/Strep). The cells were cultured at a certain condition (37 °C, 5% CO_2). The conditioned cell culture medium was obtained by soaking biomaterials in the cell culture medium for 1, 3, and 5 days. The Janus personal cooling management fabric and 3 M Nexcare Bandage as a control group were sterilized by 50% and 75% ethanol, then exposed to UV light for 30 min. and all samples were washed with PBS. Next, samples were placed in the cell culture medium (15 mL) for varying durations. NIH 3T3 cells were seeded at 2,500 cells in 96-well plates with 100 μL of conditioned medium per well, and the cells were cultured for varying durations (1, 3, and 5 days). The NIH 3T3 cells were also seeded into fibronectin-coated confocal dishes at 10,000 cells with 1 mL of conditioned medium per dish. At each time point, 10 μL of CCK-8 solution was added to each well and incubated at 37 °C for 2 h in a cell culture incubator. Afterward, the optical density of the formazan solution at a wavelength of 450 nm was determined with a microplate spectrophotometer. The CCK-8 cell viability assay was performed 1, 3, and 5 days and at least 5 replicate wells were examined for every measurement. Finally, the stained cells in confocal dishes were imaged to qualitatively analyze the cytotoxicity of different samples.

Water Vapor Transmission (WVT) Rate Tests

The WVT rate that represented the asymmetrical breathable performance of the Janus fabric was measured according to the ASTM E96 inverse wet-cup standards by using water vapor transmission test equipment (Model-HD-E702-100-4 Haida International Equipment, Guangdong, China), under constant temperatures of 5 °C, 15 °C, 25 °C, 35 °C, 45 °C, and 55 °C and relative humidities of 30%, 50%, 70%, and 90%. The WVT rate values were canlculated by $\mathrm{WVT}(\mathrm{g/m^2 \cdot 24h}) = (m_1 - m_2)/(\mathrm{S} \cdot \mathrm{t})$, ($m_1$ is the mass of the test cup before the test, m_2 is the mass of the test cup after the test, S is the actual effective area and t is the time during the testing process.)

Characterization

Optical images and movies were recorded by a digital camera (TG-6, Olympus, Japan). SEM images were obtained using a field-emission scanning electron microscope at 15 kV and an X-ray energy-dispersive spectrometer (EDS) attached to the scanning electron microscope (JEOL JSM-820) was utilized to analyze the chemical composition of the as-prepared surfaces. The thickness of the fabrics was measured by a spiral micrometer (Wenzhou Sanhe measuring instrument Co., Ltd, China). Tensile tests of fabrics were performed using an Instron 5566 tensile testing machine (Instron Ltd., High Wycombe, England). The water contact angles (WCAs) were measured with an optical video contact angle instrument (Lunderskov, Denmark) with a 5 μL distilled water droplet at ambient temperature. An infrared camera (FLIR E33) was utilized to take thermal images. The patical size distribution and the Zeta-potention were measured by Zetasizer Nano ZS, Malvern. The thermal conductivity of samples was measured by a guarded hot plate (Thermo Labo II). The stained cells in confocal dishes were imaged by Leica TCS SP8 confocal microscope (Leica Microsystems, Germany).

Supplementary Information The online version contains supplementary material available at https://doi.org/10.1007/s42765-022-00200-4.

Acknowledgements The authors gratefully acknowledge the financial support from the Contract Research ("Development of Breathable Fabrics with Nano-Electrospun Membrane", CityU ref.: 9231419), the National Natural Science Foundation of China ("Study of Multi-Responsive Shape Memory Polyurethane Nanocomposites Inspired by Natural Fibers", Grant No. 51673162), Startup Grant of CityU ("Laboratory of Wearable Materials for Healthcare", Grant No. 9380116) and National Natural Science Foundation of China, Grant No. 52073241.

Author Contributions YS and SS contributed equally to this work. JLH, YS, SS and ZCD conceived the concept together. JLH supervised the whole project throughout the writing and final proofing of the manuscript. YS and SS conducted the main experimental design and drafted the manuscript. ZCD, JQY, HBW helped with some tests and edited the manuscript. FXS helped with the theoretical analysis. All authors reviewed the manuscript and provided input.

Declarations

Conflict of interest The authors declare that there are no financial and nonfinancial competing interests.

References

1. Voosen P. Global temperatures in 2020 tied record highs. *Science* **2021**;*371*:334.
2. Eom J, Hyun M, Lee J, Lee H. Increase in household energy consumption due to ambient air pollution. *Nat Energy* **2020**;*5*:976.
3. Teitelbaum E, Chen KW, Aviv D, Bradford K, Ruefenacht L, Sheppard D, Teitelbaum M, Meggers F, Pantelic J, Rysanek A. Membrane-assisted radiant cooling for expanding thermal comfort zones globally without air conditioning. *P Natl Acad Sci USA* **2020**;*117*:21162.
4. Chen Y, Mandal J, Li W, Smith-Washington A, Tsai CC, Huang W, Shrestha S, Yu N, Han RPS, Cao A, Yang Y. Colored and paintable bilayer coatings with high solar-infrared reflectance for efficient cooling. *Sci Adv.* **2020**;*6*:eaaz5413.
5. Zeng S, Pian S, Su M, Wang Z, Wu M, Liu X, Chen M, Xiang Y, Wu J, Zhang M, Cen Q, Tang Y, Zhou X, Huang Z, Wang R, Tunuhe A, Sun X, Xia Z, Tian M, Chen M, Ma X, Yang L, Zhou J, Zhou H, Yang Q, Li X, Ma Y, Tao G. Hierarchical-morphology metafabric for scalable passive daytime radiative cooling. *Science* **2021**;*373*:692.
6. Haechler I, Park H, Schnoering G, Gulich T, Rohner M, Tripathy A, Milionis A, Schutzius TM, Poulikakos D. Exploiting radiative cooling for uninterrupted 24-hour water harvesting from the atmosphere. *Sci Adv.* **2021**;*7*:eabf3978.
7. Tan C, Dong Z, Li Y, Zhao H, Huang X, Zhou Z, Jiang JW, Long YZ, Jiang P, Zhang TY, Sun B. A high performance wearable strain sensor with advanced thermal management for motion monitoring. *Nat Commun.* **2020**;*11*:3530.
8. Luo H, Li Q, Du K, Xu Z, Zhu H, Liu D, Cai L, Ghosh P, Qiu M. An ultra-thin colored textile with simultaneous solar and passive heating abilities. *Nano Energy* **2019**;*65*:103998.
9. Luo H, Zhu Y, Xu Z, Hong Y, Ghosh P, Kaur S, Wu M, Yang C, Qiu M, Li Q. Outdoor personal thermal management with simultaneous electricity generation. *Nano Lett.* **2021**;*21*:3879.
10. Dai B, Li K, Shi L, Wan X, Liu X, Zhang F, Jiang L, Wang S. Bioinspired janus textile with conical micropores for human body moisture and thermal management. *Adv Mater.* **2019**;*31*:1904113.
11. Miao D, Wang X, Yu J, Ding B. A biomimetic transpiration textile for highly efficient personal drying and cooling. *Adv Funct Mater.* **2021**;*31*:2008705.
12. Wang Y, Liang X, Zhu H, Xin JH, Zhang Q, Zhu S. Reversible water transportation diode: temperature-adaptive smart Janus textile for moisture/thermal management. *Adv Funct Mater.* **2020**;*30*:1907851.
13. Dong Y, Zheng Y, Zhang K, Yao Y, Wang L, Li X, Yu J, Ding B. Electrospun nanofibrous materials for wound healing. *Adv Fiber Mater.* **2020**;*2*:212.
14. Zeng C, Wang H, Zhou H, Lin T. Directional water transport fabrics with durable ultra-high one-way transport capacity. *Adv Mater Interfaces* **2016**;*3*:1600036.
15. Wang H, Niu H, Zhou H, Wei X, Yang W, Lin T. Multifunctional directional water transport fabrics with moisture sensing capability. *ACS Appl Mater Interfaces* **2019**;*11*:22878.

16. Peng Y, Cui Y. Advanced textiles for personal thermal management and energy. *Joule* **2020**;*4*:724.
17. Hsu PC, Li X. Photon-engineered radiative cooling textiles. *Science* **2020**;*370*:784.
18. Hsu PC, Liu C, Song AY, Zhang Z, Peng Y, Xie J, Liu K, Wu CL, Catrysse PB, Cai L, Zhai S, Majumdar A, Fan S, Cui Y. A dual-mode textile for human body radiative heating and cooling. *Sci Adv* **2017**;*3*:e1700895.
19. Zhou L, Song H, Liang J, Singer M, Zhou M, Stegenburgs E, Zhang N, Xu C, Ng T, Yu Z, Ooi B, Gan Q. A polydimethylsiloxane-coated metal structure for all-day radiative cooling. *Nat Sustain.* **2019**;*2*:718.
20. Hu J, Iqbal MI, Sun F. Wool can be cool: water-actuating woolen knitwear for both hot and cold. *Adv Funct Mater.* **2020**;*30*:2005033.
21. Zhang XA, Yu S, Xu B, Li M, Peng Z, Wang Y, Deng S, Wu X, Wu Z, Ouyang M, Wang Y. Dynamic gating of infrared radiation in a textile. *Science* **2019**;*363*:619.
22. Iqbal MI, Sun F, Fei B, Xia Q, Wang X, Hu J. Knit architecture for water-actuating woolen knitwear and its personalized thermal management. *ACS Appl Mater Interfaces* **2021**;*13*:6298.
23. Yan W, Miao D, Babar AA, Zhao J, Jia Y, Ding B, Wang X. Multi-scaled interconnected inter-and intra-fiber porous janus membranes for enhanced directional moisture transport. *J Colloid Interface Sci.* **2020**;*565*:426.
24. Wang X, Huang Z, Miao D, Zhao J, Yu J, Ding B. Biomimetic fibrous murray membranes with ultrafast water transport and evaporation for smart moisture-wicking fabrics. *ACS Nano.* **2019**;*13*:1060.
25. Fu C, Gu L, Zeng Z, Xue Q. Simply adjusting the unidirectional liquid transport of scalable Janus membranes toward moisture-wicking fabric, rapid demulsification, and fast oil/water separation. *ACS Appl Mater Interfaces* **2020**;*12*:51102.
26. Zhou H, Guo Z. Superwetting Janus membranes: focusing on unidirectional transport behaviors and multiple applications. *J Mater Chem A* **2019**;*7*:12921.
27. Lao L, Shou D, Wu YS, Fan JT. "Skin-like" fabric for personal moisture management. *Sci Adv.* **2020**;*6*:0013.
28. Shi L, Liu X, Wang W, Jiang L, Wang S. A self-pumping dressing for draining excessive biofluid around wounds. *Adv Mater.* **2019**;*31*:1804187.
29. Zhao Y, Wang H, Zhou H, Lin T. Directional fluid transport in thin porous materials and its functional applications. *Small* **2017**;*13*:1601070.
30. Si Y, Guo C, Xu X, Zhang K, Tan R, Lau K, Hu J. Bioinspired Janus all-natural electrospinning membranes with directional water transport as ecofriendly dry facial masks. *ACS Sustainable Chem Eng.* **2022**;*10*:7726.
31. Zhou W, Yu X, Li Y, Jiao W, Si Y, Yu J, Ding B. Green-solvent-processed fibrous membranes with water/oil/dust-resistant and breathable performances for protective textiles. *ACS Appl Mater Interfaces* **2021**;*13*:2081.
32. Zhang D, Yang W, Gong W, Ma W, Hou C, Li Y, Zhang Q, Wang H. Abrasion resistant/waterproof stretchable triboelectric yarns based on fermat spirals. *Adv Mater.* **2021**;*33*:2100782.
33. Zhao J, Zhu W, Wang X, Liu L, Yu J, Ding B. Fluorine-free waterborne coating for environmentally friendly, robustly water-resistant, and highly breathable fibrous textiles. *ACS Nano* **2020**;*14*:1045.
34. Yu X, Li Y, Wang X, Si Y, Yu J, Ding B. Thermoconductive, moisture-permeable, and superhydrophobic nanofibrous membranes with interpenetrated boron nitride network for personal cooling fabrics. *ACS Appl Mater Interfaces* **2020**;*12*:32078.
35. Kamtsikakis A, Baales J, Zeisler-Diehl VV, Vanhecke D, Zoppe JO, Schreiber L, Weder C. Asymmetric water transport in dense leaf cuticles and cuticle-inspired compositionally graded membranes. *Nat Commun.* **2021**;*12*:1267.
36. Shi S, Si Y, Han Y, Wu T, Iqbal MI, Fei B, Li RKY, Hu J, Qu J. Recent progress in protective membranes fabricated via electrospinning: advanced materials, biomimetic structures, and functional applications. *Adv Mater.* **2021**;*34*:e2107938.
37. He X, Yang S, Pei Q, Song Y, Liu C, Xu T, Zhang X. Integrated smart janus textile bands for self-pumping sweat sampling and analysis. *ACS Sensors* **2020**;*5*:1548.
38. Liu RR, Hou LL, Yue GC, Li HK, Zhang JS, Liu J, Miao BB, Wang N, Bai J, Cui ZM, Liu TX, Zhao Y. Progress of fabrication and applications of electrospun hierarchically porous nanofibers. *Adv Fiber Mater.* **2022**. https://doi.org/10.1007/s42765-022-00132-z .
39. Gu H, Li G, Li P, Liu H, Chadyagondo TT, Li N, Xiong J. Superhydrophobic and breathable SiO_2/polyurethane porous membrane for durable water repellent application and oil-water separation. *Appl Surf Sci.* **2020**;*512*:144837.
40. Shi S, Han Y, Hu J. Robust waterproof and self-adaptive breathable membrane with heat retention property for intelligent protective cloth. *Prog Org Coat* **2019**;*137*:105303.
41. Tian X, Jin H, Sainio J, Ras RHA, Ikkala O. Droplet and fluid gating by biomimetic janus membranes. *Adv Funct Mater.* **2014**;*24*:6023.
42. Zheng S, Du M, Miao W, Wang D, Zhu Z, Tian Y, Jiang L. 2D prior spreading inspired from Chinese xuan papers. *Adv Funct Mater.* **2018**;*28*:1800832.
43. Si Y, Dong Z, Jiang L. Bioinspired designs of superhydrophobic and superhydrophilic materials. *ACS Cent Sci.* **2018**;*4*:1102.
44. Si Y, Wang T, Li C, Yu C, Li N, Gao C, Dong Z, Jiang L. Liquids unidirectional transport on dual-scale arrays. *ACS Nano* **2018**;*12*:9214.
45. Gennes PD, Brochard-Wyart F, Quéré D. Capillarity and wetting phenomena: drops, bubbles, pearls, waves. Berlin: Springer Science & Business Media; **2013**.
46. Tian X, Li J, Wang X. Anisotropic liquid penetration arising from a cross-sectional wettability gradient. *Soft Matter.* **2012**;*8*:2633.
47. Zhou W, Gong X, Li Y, Si Y, Zhang S, Yu J, Ding B. Waterborne electrospinning of fluorine-free stretchable nanofiber membranes with waterproof and breathable capabilities for protective textiles. *J Colloid Interface Sci.* **2021**;*602*:105.
48. Liu K, Deng L, Zhang T, Shen K, Wang X. Facile fabrication of environmentally friendly, waterproof, and breathable nanofibrous membranes with high UV-resistant performance by one-step electrospinning. *Ind Eng Chem Res.* **2020**;*59*:4447.
49. Zhao J, Zhu W, Yan W, Wang X, Liu L, Yu J, Ding B. Tailoring waterproof and breathable properties of environmentally friendly electrospun fibrous membranes by optimizing porous structure and surface wettability. *Compos Commun.* **2019**;*15*:40.
50. Gu J, Gu H, Zhang Q, Zhao Y, Li N, Xiong J. Sandwich-structured composite fibrous membranes with tunable porous structure for waterproof, breathable, and oil-water separation applications. *J Colloid Interface Sci.* **2018**;*514*:386.
51. Ahmed Babar A, Zhao X, Wang X, Yu J, Ding B. One-step fabrication of multi-scaled, inter-connected hierarchical fibrous membranes for directional moisture transport. *J Colloid Interface Sci.* **2020**;*577*:207.
52. Miao D, Huang Z, Wang X, Yu J, Ding B. Continuous, spontaneous, and directional water transport in the trilayered fibrous membranes for functional moisture wicking textiles. *Small* **2018**;*14*:1801527.
53. Dhyani A, Wang J, Halvey AK, Macdonald B, Mehta G, Tuteja A. Design and applications of surfaces that control the accretion of matter. *Science* **2021**;*373*:eaba5010.

54. Wang D, Sun Q, Hokkanen MJ, Zhang C, Lin FY, Liu Q, Zhu SP, Zhou T, Chang Q, He B, Zhou Q, Chen L, Wang Z, Ras RHA, Deng X. Design of robust superhydrophobic surfaces. *Nature* **2020**;*582*:55.
55. Su Y, Fan T, Cui W, Li Y, Ramakrishna S, Long Y. Advanced electrospun nanofibrous materials for efficient oil/water separation. *Adv Fiber Mater.* **2022**. https://doi.org/10.1007/s42765-022-00158-3 .
56. Xiao R, Hou C, Yang W, Su Y, Li Y, Zhang Q, Gao P, Wang H. Infrared-radiation-enhanced nanofiber membrane for sky radiative cooling of the human body. *ACS Appl Mater Interfaces* **2019**;*11*:44673.
57. Fan J, Luo Z, Li Y. Heat and moisture transfer with sorption and condensation in porous clothing assemblies and numerical simulation. *Int J Heat Mass Transf.* **2000**;*43*:2989.
58. Wang Y, Xia G, Yu H, Qian B, Cheung YH, Wong LH, Xin JH. Mussel-inspired design of a self-adhesive agent for durable moisture management and bacterial inhibition on PET fabric. *Adv Mater.* **2021**;*33*:2100140.
59. Yang X, Li L, Yang D, Nie J, Ma G. Electrospun core-shell fibrous 2D scaffold with biocompatible poly(glycerol sebacate) and poly-L-lactic acid for wound healing. *Adv Fiber Mater.* **2020**;*2*:105.
60. Liang Y, He J, Guo B. Functional hydrogels as wound dressing to enhance wound healing. *ACS Nano* **2021**;*15*:12687.